

This discussion paper is/has been under review for the journal Biogeosciences (BG).
Please refer to the corresponding final paper in BG if available.

Deriving seasonal dynamics in ecosystem properties of semi-arid savannas using in situ based hyperspectral reflectance

T. Tagesson¹, R. Fensholt¹, S. Huber², S. Horion¹, I. Guiro³, A. Ehammer¹, and J. Ardö⁴

¹Department of Geosciences and Natural Resource Management, University of Copenhagen, Øster Voldgade 10, 1350 Copenhagen, Denmark

²Danish Hydrological Institute, DHI GRAS A/S, Agern Allé 5, 2970 Hørsholm, Denmark

³Laboratoire d'Enseignement et de Recherche en Géomatique, Ecole Supérieure Polytechnique, Université Cheikh Anta Diop de Dakar, BP 25275 Dakar-Fann, Senegal

⁴Department of Physical Geography and Ecosystem Science, Lund University, Sölvegatan 12, 223 62 Lund, Sweden

Received: 11 December 2014 – Accepted: 15 January 2015 – Published: 20 February 2015

Correspondence to: T. Tagesson (torbern.tagesson@ign.ku.dk)

Published by Copernicus Publications on behalf of the European Geosciences Union.

Title Page

Abstract

Introduction

Conclusions

References

Tables

Figures



Back

Close

Full Screen / Esc

Printer-friendly Version

Interactive Discussion



Abstract

This paper investigates how seasonal hyperspectral reflectance data (between 350 and 1800 nm) can be used to infer ecosystem properties for a semi-arid savanna ecosystem in West Africa using a unique in situ based dataset. Relationships between seasonal dynamics in hyperspectral reflectance, and ecosystem properties (biomass, gross primary productivity (GPP), light use efficiency (LUE), and fraction of photosynthetically active radiation absorbed by vegetation (FAPAR)) were analysed. Reflectance data (ρ) were used to study the relationship between normalised difference spectral indices (NDSI) and the measured ecosystem properties. Finally, also the effects of variable sun sensor viewing geometry on different NDSI wavelength combinations were analysed. The wavelengths with the strongest correlation to seasonal dynamics in ecosystem properties were shortwave infrared (biomass), the peak absorption band for chlorophyll *a* and *b* (at 682 nm) (GPP), the oxygen A-band at 761 nm used for estimating chlorophyll fluorescence (GPP, and LUE), and blue wavelengths (FAPAR). The NDSI with the strongest correlation to: (i) biomass combined red edge reflectance (ρ_{705}) with green reflectance (ρ_{587}), (ii) GPP combined wavelengths at the peak of green reflection (ρ_{518} , ρ_{556}), (iii) the LUE combined red (ρ_{688}) with blue reflectance (ρ_{436}), and (iv) FAPAR combined blue (ρ_{399}) and near infrared (ρ_{1295}) wavelengths. NDSI combining near infrared and shortwave infrared were strongly affected by solar zenith angles and sensor viewing geometry, as were many combinations of visible wavelengths. This study provides analyses based upon novel multi-angular hyperspectral data for validation of Earth Observation based properties of semi-arid ecosystems, as well as insights for designing spectral characteristics of future sensors for ecosystem monitoring.

BGD

12, 3315–3347, 2015

Hyperspectral reflectance of semi-arid savannas

T. Tagesson et al.

Title Page

Abstract

Introduction

Conclusions

References

Tables

Figures



Back

Close

Full Screen / Esc

Printer-friendly Version

Interactive Discussion



1 Introduction

Hyperspectral measurements of the Earth's surface provide relevant information for many ecological applications. An important tool for spatial extrapolation of ecosystem functions and properties is to study how spectral properties are related to in situ measured ecosystem properties. These relationships found the basis for up-scaling using earth observation (EO) data. Continuous in situ measurements are thereby essential for improving our understanding of the functioning of the observed ecosystems. Strong relationships have for example been found between information in the reflectance spectrum and ecosystem properties such as, leaf area index (LAI), fraction of photosynthetically active radiation (PAR) absorbed by the vegetation (FAPAR), light use efficiency (LUE), biomass, vegetation primary productivity, nitrogen and chlorophyll content, and vegetation water content (e.g. Thenkabail et al., 2012; Tagesson et al., 2009; Gower et al., 1999; Sjöström et al., 2009; Sims and Gamon, 2003). In situ observations of spectral reflectance are also important for parameterisation and validation of canopy reflectance models, and space and airborne products (Coburn and Peddle, 2006). Even though in situ measurements are fundamental for the EO research community, such datasets are still rare and at the present state they do not cover different biomes at the global scale (Huber et al., 2014).

There are many methods for analysing relationships between hyperspectral reflectance and ecosystem properties, such as multivariate methods, derivative techniques, and radiative transfer modelling (Bowyer and Danson, 2004; Ceccato et al., 2002; Danson et al., 1992; Roberto et al., 2012). Still, due to its simplicity, the combination of reflectance into vegetation indices is the major method for up-scaling using EO data. By far, the most commonly applied vegetation indices are the ratio type of indices, e.g. the normalised difference vegetation index (NDVI), which is calculated by dividing the difference in the reflectance in the near infrared (ρ_{NIR}) and red (ρ_{red}) wavelength bands by the sum of ρ_{NIR} and ρ_{red} (Tucker, 1979; Rouse et al., 1974). The near infrared (NIR) radiance is strongly scattered by the air–water interfaces between

BGD

12, 3315–3347, 2015

Hyperspectral reflectance of semi-arid savannas

T. Tagesson et al.

Title Page

Abstract

Introduction

Conclusions

References

Tables

Figures



Back

Close

Full Screen / Esc

Printer-friendly Version

Interactive Discussion



the cells whereas red radiance is absorbed by chlorophyll and its accessory pigments (Gates et al., 1965). The normalization with the sum in the denominator is a mean to reduce the effects of solar zenith angle, sensor viewing geometry, and atmospheric errors as well as enhancing the signal of the observed target (e.g. Qi et al., 1994; Inoue et al., 2008).

Wavelength specific spectral reflectance is known to be related to leaf characteristics such as chlorophyll concentration, dry matter content, internal structure parameter and equivalent water thickness (Ceccato et al., 2002). Hyperspectral reflectance data can be combined into a matrix of normalised difference spectral indices (NDSI), following the NDVI rationing approach. Correlating the NDSI with ecosystem properties provides a way for an improved empirically based understanding of the relationship between information in the reflectance spectrum with ground surface properties (e.g. Inoue et al., 2008). Several studies have analysed relationships between hyperspectral reflectance, NDSI, and ecosystem properties (e.g. Thenkabail et al., 2000, 2012; Cho et al., 2007; Psomas et al., 2011; Inoue et al., 2008; Gamon et al., 1992; Feret et al., 2008). Still, it is extremely important to examine these relationships for different ecosystems across the earth and investigate their applicability for different environmental conditions and under different effects of biotic and abiotic stresses.

A strong correlation between an NDSI and an ecosystem property does not necessarily indicate that the NDSI is a good indicator of vegetation conditions to be applied to EO systems. Visible, NIR and shortwave infrared (SWIR) have different sensitivity to variations in solar zenith angles, stand structure, environmental conditions and sensor viewing geometry. The influence from sun-sensor variations on the reflected signal has been studied using radiative transfer models (e.g. Jacquemoud et al., 2009). However, effects of variable sun angles and sensor viewing geometries are not well documented for different plant functional types of natural ecosystems except for individual controlled experiments based on the use of field goniometers (Sandmeier et al., 1998). Improved knowledge regarding the influence from sun-

BGD

12, 3315–3347, 2015

Hyperspectral reflectance of semi-arid savannas

T. Tagesson et al.

[Title Page](#)

[Abstract](#)

[Introduction](#)

[Conclusions](#)

[References](#)

[Tables](#)

[Figures](#)



[Back](#)

[Close](#)

[Full Screen / Esc](#)

[Printer-friendly Version](#)

[Interactive Discussion](#)



sensor variability on different NDSI combinations is thereby essential for validating the applicability of an NDSI for EO up-scaling purposes.

The Dahra field site in Senegal, West Africa, was established in 2002 as an in situ research site to improve our knowledge regarding properties of semi-arid savanna ecosystems and their responses to climatic and environmental changes (Tagesson et al., 2014). A strong focus of this instrumental setup is to gain insight into the relationships between ground surface reflectance and savanna ecosystem properties for EO up-scaling purposes. This paper presents a unique in situ dataset of seasonal dynamics in hyperspectral reflectance and demonstrates how seasonal dynamics in hyperspectral reflectance can be used to describe the seasonal dynamics in ecosystem properties of semi-arid savanna ecosystems. The objectives are threefold: (i) to quantify the relationship between seasonal dynamics of in situ hyperspectral reflectance between 350 and 1800 nm and ecosystem properties (biomass, gross primary productivity (GPP), LUE, and FAPAR), (ii) to quantify the relationship between NDSI with different wavelength combinations (350–1800 nm) and the measured ecosystem properties, (iii) to analyse and quantify effects of variable sun angles and sensor viewing geometries on different NDSI combinations.

2 Materials and method

2.1 Site description

All measurements used for the present study were conducted at the Dahra field site in the Sahelian ecoclimatic zone north-east of the town Dahra in the semi-arid central part of Senegal (15°24'10" N, 15°25'56" W) during 2011 and 2012. Rainfall is sparse in the region with a mean annual sum of 416 mm (1951–2003). More than 95% of the rain falls between July and October, with August being the wettest month. The mean annual air temperature is 29 °C (1951–2003), May is the warmest and January is the coldest month with mean monthly temperature of 32 and 25 °C, respectively.

BGD

12, 3315–3347, 2015

Hyperspectral reflectance of semi-arid savannas

T. Tagesson et al.

Title Page

Abstract

Introduction

Conclusions

References

Tables

Figures



Back

Close

Full Screen / Esc

Printer-friendly Version

Interactive Discussion



Hyperspectral reflectance of semi-arid savannas

T. Tagesson et al.

Title Page

Abstract

Introduction

Conclusions

References

Tables

Figures



Back

Close

Full Screen / Esc

Printer-friendly Version

Interactive Discussion



The Dahra site has a short growing season (~ 3 months), following the rainy season with leaf area index generally ranging between 0 and 2 (Fensholt et al., 2004). The area is dominated by annual grasses (e.g. *Schoenefeldia gracilis*, *Digitaria gayana*, *Dactyloctenium aegypticum*, *Aristida mutabilis* and *Cenchrus biflorues*) (Mbow et al., 2013) and trees and shrubs (e.g. *Acacia senegalensis* and *Balanites aegyptiaca*) are relatively sparse ($\sim 3\%$, of the land cover) (Rasmussen et al., 2011). A thorough description of the Dahra field site is given in Tagesson et al. (2014).

2.2 Meteorological and vegetation variables

At the Dahra field site, a range of meteorological variables have been measured for more than ten years: air temperature ($^{\circ}\text{C}$) and relative humidity (%) were measured at 2 m height; soil temperature ($^{\circ}\text{C}$) and soil moisture (volumetric water content ($\text{m}^3 \text{m}^{-3} \times 100$) (%)) were collected at 0.05 m depths; rainfall (mm) was measured at 2 m height; incoming ($_{\text{inc}}$) and reflected ($_{\text{ref}}$) PAR ($\mu\text{mol m}^{-2} \text{s}^{-1}$) was measured at 10.5 m height, and PAR transmitted through the vegetation ($\text{PAR}_{\text{transmit}}$) was measured at 6 plots at ~ 0.01 m height (Tagesson et al., 2014). PAR absorbed by the vegetation (APAR) was estimated by:

$$\text{APAR} = \text{PAR}_{\text{inc}} - \text{PAR}_{\text{ref}} - (1 - \text{albedo}_{\text{soil}}) \cdot \text{PAR}_{\text{transmit}} \quad (1)$$

and FAPAR was estimated by dividing APAR with PAR_{inc} (Tagesson et al., 2014).

The total above ground green biomass (g m^{-2}) of the herbaceous vegetation was sampled approximately every 10 days during the growing seasons 2011 and 2012 at 28 one m^2 plots located along two ~ 1060 m long transects (Mbow et al., 2013). The study area is flat and characterised by homogenous grassland savanna and the conditions in these sample plots are generally found to be representative for the conditions in the entire measurement area (Fensholt et al., 2006). All above ground green herbaceous vegetation matter was collected and weighed in the field to get the fresh weight. The dry matter (DW) was estimated by oven-drying the green biomass.

For a thorough description regarding the biomass sampling we refer to Mbow et al. (2013).

2.3 Estimates of gross primary productivity and light use efficiency

Net ecosystem exchange of CO₂ (NEE) ($\mu\text{molCO}_2\text{m}^{-2}\text{s}^{-1}$) was measured with an eddy covariance system, consisting of an open path infrared gas analyser (LI-7500, LI-COR Inc., Lincoln, USA) and a 3-axis sonic anemometer (GILL instruments, Hampshire, UK) from 18 July 2011 until 31 December 2012. The sensors were mounted 9 m above the ground and data were sampled at 20 Hz rate. For a thorough description of the post processing of the raw eddy covariance data, see Tagesson et al. (2014).

The daytime NEE was partitioned to GPP and ecosystem respiration using the Mysterlich light response function against PAR_{inc} (Falge et al., 2001). A 7 day moving window with one day time steps was used when fitting the functions. By subtracting dark respiration (R_d) from the light response function, it was forced through 0, and GPP was estimated:

$$\text{GPP} = -(F_{\text{csat}} + R_d) \cdot \left(1 - e^{\left(\frac{-\alpha \times \text{PAR}_{\text{inc}}}{F_{\text{csat}} + R_d} \right)} \right) \quad (2)$$

where F_{csat} is the CO₂ uptake at light saturation ($\mu\text{molCO}_2\text{m}^{-2}\text{s}^{-1}$), and α is the quantum efficiency or the initial slope of the light response curve ($\mu\text{molCO}_2(\mu\text{mol photons})^{-1}$) (Falge et al., 2001). VPD limits GPP and to account for this effect, the F_{csat} parameter was set as an exponentially decreasing function:

$$F_{\text{csat}} = \begin{cases} F_{\text{csat}} \cdot e^{-k(\text{VPD} - \text{VPD}_0)} & \text{VPD} > \text{VPD}_0 \\ F_{\text{csat}} & \text{VPD} < \text{VPD}_0 \end{cases} \quad (3)$$

where VPD₀ is 10 hPa following the method by Lasslop et al. (2010).

BGD

12, 3315–3347, 2015

Hyperspectral reflectance of semi-arid savannas

T. Tagesson et al.

Title Page

Abstract

Introduction

Conclusions

References

Tables

Figures



Back

Close

Full Screen / Esc

Printer-friendly Version

Interactive Discussion



Gaps in GPP less or equal to three days were filled with three different methods: (i) gaps shorter than two hours were filled using linear interpolation, (ii) daytime gaps were filled by using the light-response function for the 7 day moving windows, (iii) remaining gaps were filled by using mean diurnal variation 7 days moving windows (Falge et al., 2001). A linear regression model was fitted between daytime GPP and APAR for each 7 day moving window to estimate LUE, where LUE is the slope of the line.

2.4 Hyperspectral reflectance measurements and NDSI estimates

Ground surface reflectance spectra were measured every 15 min between sunrise and sunset from 15 July 2011 until 31 December 2012 using two FieldSpec3 spectrometers (ASD Inc., Colorado, USA). The spectroradiometers cover the spectral range from 350 to 1800 nm and have an instantaneous field of view of 25°. One sensor head was mounted 10.5 m above the surface providing measurements from the land surface in seven different viewing angles (nadir, 15, 30, 45° off-nadir angles towards east and west). The second sensor head was used for full-sky-irradiance measurements. The spectral reflectance was derived by estimating the ratio between the ground surface radiance and full sky irradiance. For a complete description/illustration of the spectroradiometer set up, the measurement sequence and the quality control, see Huber et al. (2014). NDSI using all possible combinations of two separate wavelengths were calculated as:

$$\text{NDSI} = \frac{(\rho_i - \rho_j)}{(\rho_i + \rho_j)} \quad (4)$$

where ρ_i and ρ_j are the daily median reflectance in two separate single wavelengths (i and j) between 350 and 1800 nm.

BGD

12, 3315–3347, 2015

Hyperspectral reflectance of semi-arid savannas

T. Tagesson et al.

Title Page

Abstract

Introduction

Conclusions

References

Tables

Figures

⏪

⏩

◀

▶

Back

Close

Full Screen / Esc

Printer-friendly Version

Interactive Discussion



2.5 Effects of varying sun and sensor viewing geometry on NDSI

The effects of variable solar zenith angles on different NDSI combinations were studied with nadir measurements taken over 15 days during the peak of the growing season in 2011 (day of year 237–251). Only days with full data coverage were used (12 of the 15 days) in order not to include bias in the results from days with incomplete datasets. The median reflectance was calculated for each wavelength for every 15 min between 08:00 and 18:00 LT. These reflectance values were combined into NDSI with different wavelength combinations. Finally, daily mean and standard deviation (SD) for all wavelength combinations were calculated. Diurnal variability in the NDSI was assessed with the coefficient of variation (COV), which is the ratio between the SD and the mean. The COV gives an indication of effects related to variable solar zenith angles.

The anisotropy factor (ANIF) was used to capture directional effects in the NDSI related to the variable view zenith angles (15, 30, 45° off-nadir angles towards east and west). The ANIF is defined as the fraction of a reflected property at a specific view direction relative to the nadir:

$$\text{ANIF}(\lambda, \theta) = \frac{\text{NDSI}(\lambda, \theta)}{\text{NDSI}_0(\lambda)} \quad (5)$$

where $\text{NDSI}(\lambda, \theta)$ is NDSI for the different wavelengths (λ) and the different viewing angles (θ), and $\text{NDSI}_0(\lambda)$ is the nadir measured NDSI (Sandmeier et al., 1998). The NDSI was calculated from median reflectance values from the peak of the growing season 2011 (day of year 237–251) and only data measured between 12:00 and 14:00 LT were used to avoid effects of variable solar zenith angles.

BGD

12, 3315–3347, 2015

Hyperspectral reflectance of semi-arid savannas

T. Tagesson et al.

Title Page

Abstract

Introduction

Conclusions

References

Tables

Figures



Back

Close

Full Screen / Esc

Printer-friendly Version

Interactive Discussion



2.6 Relationship between hyperspectral reflectance, NDSI and ecosystem properties

We examined the relationship between predictor variables (daily median hyperspectral reflectance, and NDSI from nadir observations) and response variables (biomass, GPP, LUE, and FAPAR) using linear regression analysis. We used a reduced major axis linear regression to account for errors in both the predictor and response variables. In order to estimate the robustness of the empirical relationships, we used a bootstrap simulation methodology, where the datasets were copied 200 times (Richter et al., 2012). The runs generated 200 sets of slopes, intercepts, coefficients of determination (R^2), and root-mean-square-errors (RMSE), from which median and SD was estimated. Median was used instead of average since it gives the most common model output and hereby more robust against outliers. Within the regression analysis all variables used were repeated observations of the same measurement plot. The dependent and independent variables are thereby temporally auto-correlated and cannot be regarded as statistically independent. We thereby choose not to present any statistical significance. The analyses, however, still indicate how closely coupled the explanatory variables are with the ecosystem properties.

A filter was created for the analysis between NDSI and ecosystem properties; all NDSI combinations with a COV higher than 0.066 and all NDSI combinations with ANIF values higher than 1.2 and lower than 0.8 were filtered. The COV threshold of 0.066 was used since 99.9% of the values vary less than 20% due to effects of variable solar zenith angles. Additionally, the water absorption band (1300–1500 nm) was filtered as it is strongly sensitive to atmospheric water content, and is less suitable for spatial extrapolation of ecosystem properties using air/space borne sensors (Asner, 1998). Finally, NDSI combinations including wavelengths between 350 and 390 nm were filtered owing to low signal to noise ratio in the ASD sensors (Thenkabail et al., 2004).

BGD

12, 3315–3347, 2015

Hyperspectral reflectance of semi-arid savannas

T. Tagesson et al.

Title Page

Abstract

Introduction

Conclusions

References

Tables

Figures



Back

Close

Full Screen / Esc

Printer-friendly Version

Interactive Discussion



3 Results

3.1 Seasonal dynamics in meteorological variables, ecosystem properties and hyperspectral reflectance

Daily average air temperature at 2 m height ranged between 18.4 and 37.8 °C, with low values during winter and peak values in the end of the dry season (Fig. 2a). Yearly rainfall was 486 and 606 mm for 2011 and 2012, respectively. Soil moisture ranged between 1.9 and 14.1 %, and it clearly followed the rainfall patterns (Fig. 2b and c). The CO₂ fluxes were low during the dry period and high during the rainy season (July–October) (Fig. 2e). The LUE followed GPP closely (Fig. 2f). FAPAR was low at the start of the rainy season, followed by a maximum towards the end of the rainy season, and then slowly decreased over the dry season (Fig. 2g).

The range in reflectance is large across the spectral space, and would hide the seasonal dynamics in hyperspectral reflectance if directly shown. Therefore, to clearly illustrate the seasonal dynamics in hyperspectral reflectance, the ratio between daily median nadir reflectance and the average reflectance for the entire measurement period was calculated for each wavelength (350–1800 nm). This gives a fraction of how the reflectance for each wavelength varies over the measurement period in relation to the average of the entire period (Fig. 2d). In the visible (VIS) part of the reflectance spectrum (350–700 nm) there was a stronger absorption during the second half of the rainy season and at the beginning of the dry season than during the main part of the dry season and the start of the rainy season. There was stronger NIR absorption (700–1300 nm) in the end of the rainy season and the beginning of the dry season, whereas the absorption decreased along with the dry season. Strong seasonal variation was observed in the water absorption region around 1400 nm following the succession of rainy and dry seasons. Reflectance in the short-wave infrared (SWIR; 1400–1800 nm) generally followed the seasonal dynamics of the visible part of the spectrum.

BGD

12, 3315–3347, 2015

Hyperspectral reflectance of semi-arid savannas

T. Tagesson et al.

Title Page

Abstract

Introduction

Conclusions

References

Tables

Figures



Back

Close

Full Screen / Esc

Printer-friendly Version

Interactive Discussion



3.2 Effects of sensor viewing geometry and variable sun angles on NDSI

The most pronounced effects of solar zenith angles at the peak of the growing season 2011 were observed for NDSI combining SWIR and NIR wavelengths, and with VIS wavelengths between 550 and 700 nm ($n = 576$) (Fig. 3). Remaining VIS wavelengths were mostly affected by solar zenith angles when combined with the water absorption wavelengths around 1400 nm. The same effects were seen for the view zenith angles; the strongest effects were seen for NDSI with SWIR and NIR combinations, and VIS wavelengths between 550 and 700 nm (Fig. 4). Remaining VIS wavelengths were less affected. It was also clear that ground surface anisotropy increased strongly as a function of increasing viewing angle (Fig. 4). Moreover, some band combinations showed already angular sensitivity at view zenith angles of 15° , while other band combinations only manifest anisotropic behaviour with higher view angles. Some band combinations, however, do not show any increased anisotropy at all (areas coloured in green in all three plots).

3.3 Relationship between hyperspectral reflectance, NDSI and ecosystem properties

3.3.1 Biomass

Reflectance values for all wavelengths except the water absorption band at 1100 nm were strongly correlated to biomass (Fig. 5a). The strongest correlation was found at ρ_{1675} (median ± 1 SD; $r = -0.88 \pm 0.09$), but biomass was almost equally well correlated to blue, red and NIR wavelengths. Negative correlations indicate that the more biomass the higher the absorption and hence the lower the reflectance.

NDSI combinations with reflectance in the red edge ($\rho_{680} - \rho_{750}$) and reflectance in the VIS region explained seasonal dynamics in biomass well (Fig. 6a). The strongest relationship ($R^2 = 0.88 \pm 0.07$; RMSE = 28.4 ± 8.7 gDW m $^{-2}$) between NDSI

BGD

12, 3315–3347, 2015

Hyperspectral reflectance of semi-arid savannas

T. Tagesson et al.

Title Page

Abstract

Introduction

Conclusions

References

Tables

Figures



Back

Close

Full Screen / Esc

Printer-friendly Version

Interactive Discussion



and biomass was found for NDSI combining 705 and 587 nm (NDSI[705, 587]) (Table 1, Fig. 7a).

3.3.2 Gross primary productivity

The relationship between GPP and nadir measured hyperspectral reflectance is inverted as compared to other correlation coefficient lines (Fig. 5b), since GPP is defined as a withdrawal of CO₂ from the atmosphere with higher negative values for a larger CO₂ uptake. The seasonal dynamics in GPP was strongly positively correlated to reflectance in the blue, red, SWIR wavelengths, and the water absorption band at 1100nm whereas it was strongly negatively correlated to the NIR reflectance. The study revealed the strongest positive and negative correlations for reflectance at 682 nm ($r = 0.70 \pm 0.02$) and 761 nm ($r = -0.74 \pm 0.02$), respectively. NDSI combinations that explained most of the GPP variability were different combinations of the VIS and NIR or red and SWIR wavelengths (Fig. 6b). However, the strongest relationship was seen at NDSI[518, 556] ($R^2 = 0.86 \pm 0.02$; RMSE = $1.5 \pm 0.1 \text{ g C m}^{-2} \text{ day}^{-1}$) (Table 1; Fig. 7b).

3.3.3 Light use efficiency

LUE was negatively correlated with reflectance in the blue, and red spectral ranges and in the water absorption band at 1100nm and it was positively correlated in the NIR wavelengths (Fig. 5c). Reflectance at 761 nm yielded the strongest positive correlation ($r = 0.87 \pm 0.01$). When combining the different wavelengths to NDSI, the VIS wavelengths explained variation in LUE well, with the strongest relationships in the red and blue parts of the spectrum (Fig. 6c). LUE correlated most strongly with NDSI[436, 688] ($R^2 = 0.81 \pm 0.02$; RMSE = $0.26 \pm 0.02 \text{ g C MJ}^{-1}$) (Table 1; Fig. 7c).

BGD

12, 3315–3347, 2015

Hyperspectral reflectance of semi-arid savannas

T. Tagesson et al.

Title Page

Abstract

Introduction

Conclusions

References

Tables

Figures



Back

Close

Full Screen / Esc

Printer-friendly Version

Interactive Discussion



3.3.4 Fraction of photosynthetically active radiation absorbed by the vegetation

FAPAR was negatively correlated to nadir measured reflectance for most wavelengths (Fig. 5d); the higher FAPAR the higher the absorption, and thereby the lower the reflectance. The strongest correlation was found at a blue wavelength ρ_{412} ($r = -0.92 \pm 0.01$). When wavelengths were combined to NDSI, combining violet/blue with NIR and SWIR wavelengths generated the NDSI with the strongest relationships (Fig. 6d) with a maximum R^2 of 0.81 ± 0.02 (RMSE = 0.059 ± 0.003) for NDSI[399, 1295] (Table 1; Fig. 7d).

4 Discussion

4.1 Effects of sensor viewing geometry and variable sun angles on the NDSI

Effects of solar zenith angles and sensor viewing geometry were similar (Figs. 3 and 4), since they affect reflectance measurements in a similar way (Kimes, 1983). In dense and erectophile canopies, reflectance increases with sensor viewing and solar zenith angles, because a larger fraction of the upper vegetation canopy is viewed/illuminated, whereas the shadowed lower part of the canopy contributes less to the measured signal as shown previously by several studies (Huete et al., 1992; Jin et al., 2002; Huber et al., 2014; Kimes, 1983). However, the radiative transfer within a green canopy is complex, and differs across the spectral region (Huber et al., 2014). Less radiation is available for scattering of high absorbing spectral ranges (such as the VIS wavelengths), and this tends to increase the contrast between shadowed and illuminated areas for these wavelengths, whereas in the NIR and SWIR ranges, more radiation is scattered and transmitted, which thereby decreases the difference between shadowed and illuminated areas within the canopy (Kimes, 1983; Hapke et al., 1996). A recognised advantage of NDSI calculations is that errors/biases being similar in both wavelengths included in the index are suppressed by the normalisation. However, for

BGD

12, 3315–3347, 2015

Hyperspectral reflectance of semi-arid savannas

T. Tagesson et al.

Title Page

Abstract

Introduction

Conclusions

References

Tables

Figures



Back

Close

Full Screen / Esc

Printer-friendly Version

Interactive Discussion



Hyperspectral reflectance of semi-arid savannas

T. Tagesson et al.

[Title Page](#)

[Abstract](#)

[Introduction](#)

[Conclusions](#)

[References](#)

[Tables](#)

[Figures](#)



[Back](#)

[Close](#)

[Full Screen / Esc](#)

[Printer-friendly Version](#)

[Interactive Discussion](#)



a given situation where errors/biases are different for the wavelengths used, such as effects generated by sun-sensor geometry, it will affect the value of the index. This is especially the case for low index values (closer to 0) whereas larger index values (closer to 1 and -1) become less sensitive. The relative reflectance difference between NIR and SWIR is lower as compared to indices including the VIS domain; NIR/SWIR based indices thereby generate lower NDSI values with higher sensitivity to sun-sensor geometry generated differences between included wavelengths (Figs. 3 and 4).

The importance of directional effects for the applicability of normalized difference spectral indices has been pointed out as an issue in numerous papers (e.g. Holben and Fraser, 1984; van Leeuwen et al., 1999; Cihlar et al., 1994; Fensholt et al., 2010; Gao et al., 2002). This study confirms these challenges for NIR/SWIR based indices, but the results also indicate several wavelength combinations from which these effects are less severe and potentially applicable to EO data without disturbance from viewing/illumination geometry for this type of vegetation. Additionally, multi-angular reflectance data provide accurate and extra information of e.g. canopy structure, photosynthetic efficiency and capacity (Bicheron and Leroy, 2000; Asner, 1998; Pisek et al., 2013), and this unique in situ based multi-angular high temporal resolution dataset may thus be used for future research of canopy radiative transfer. The multi-angular dataset is also highly valuable for evaluation and validation of satellite based products, where the separation of view angle and atmospheric effects can only be done using radiative transfer models (Holben and Fraser, 1984).

4.2 Seasonal dynamics in hyperspectral reflectance, NDSI and ecosystem properties

4.2.1 Biomass

The strong correlation between biomass and the majority of the reflectance spectrum indicates the strong effects of phenology on the seasonal dynamics in the reflectance spectra (Fig. 5a). Variability in VIS (350–700 nm) reflectance for vegetated areas is

Hyperspectral reflectance of semi-arid savannas

T. Tagesson et al.

Title Page

Abstract

Introduction

Conclusions

References

Tables

Figures



Back

Close

Full Screen / Esc

Printer-friendly Version

Interactive Discussion



strongly related to changes in leaf pigments (Asner, 1998), and this can also be seen in Fig. 2d since absorption was much stronger during the rainy (growing) season, than during the dry season. To avoid overheating a large fraction of NIR radiation is reflected in green healthy vegetation and NIR reflectance is mostly affected by changes in LAI, canopy architecture, and by the spongy mesophyll layer in green leaves (Asner, 1998). Several studies have shown that biomass accumulation increases ecosystem water content, which thereby increases SWIR absorption (e.g. Psomas et al., 2011; Asner, 1998). We found the strongest correlation for biomass with a SWIR wavelength thereby confirming the studies by Lee (2004) and Psomas et al. (2011) in that SWIR wavelengths are good predictors of LAI or biomass.

The NDVI is known to saturate at high biomass because the absorption of red light at ~ 670 nm reaches a peak at higher biomass loads whereas the NIR reflectance continues to increase due to multiple scattering effects (Mutanga and Skidmore, 2004; Jin and Eklundh, 2014). Several studies have shown that NDSI computed with narrowband reflectance improve this relationship, for example using shorter and longer wavelengths of the red edge (700–780 nm) (Cho et al., 2007; Mutanga and Skidmore, 2004; Lee, 2004), and NIR and SWIR wavelengths (Psomas et al., 2011; Lee, 2004). The NDSI with the strongest correlation to biomass was computed using red edge reflectance (ρ_{705}) and green reflectance (ρ_{587}). Vegetation stress and information about chlorophyll and nitrogen status of plants can be extracted from the red-edge region (Gitelson et al., 1996). Wavelengths around ρ_{550} are located right at the peak of green reflection and closely related to the total chlorophyll content, leaf nitrogen content, and chlorophyll/carotenoid ratio and have previously been shown to be closely related to biomass (Inoue et al., 2008; Thenkabail et al., 2012).

4.2.2 Gross primary productivity

The maximum absorption in the red wavelengths generally occurs at 682 nm as this is the peak absorption for chlorophyll *a* and *b* (Thenkabail et al., 2000), and this was also the wavelength being most strongly correlated with GPP. Reflectance at 682 nm

Hyperspectral reflectance of semi-arid savannas

T. Tagesson et al.

[Title Page](#)

[Abstract](#)

[Introduction](#)

[Conclusions](#)

[References](#)

[Tables](#)

[Figures](#)



[Back](#)

[Close](#)

[Full Screen / Esc](#)

[Printer-friendly Version](#)

[Interactive Discussion](#)



was previously shown to be strongly related to LAI, biomass, plant height, NPP, and crop type discrimination (Thenkabail et al., 2004, 2012). The NDSI with the strongest relationship to GPP was based on reflectance in the vicinity of the green peak. The photochemical reflectance index (PRI) normalizes reflectance at 531 and 570 nm and it was suggested for detection of diurnal variation in the xanthophyll cycle activity (Gamon et al., 1992), and it is commonly used for estimating productivity efficiency of the vegetation (e.g. Soudani et al., 2014). The present study thereby confirms the strong applicability of the wavelengths in the vicinity of the green peak for vegetation productivity studies. Again, wavelengths around the green peak are related to the total chlorophyll content, leaf nitrogen content, chlorophyll/carotenoid ratio, and biomass (Inoue et al., 2008; Thenkabail et al., 2012).

4.2.3 Light use efficiency

Both LUE and GPP were most strongly correlated with reflectance at 761 nm, which is the oxygen A-band within the NIR wavelengths. Reflectance at 761 nm is commonly used for estimating solar-induced chlorophyll fluorescence due to radiation emitted by the chlorophyll, and it has been suggested as a direct measure of health status of the vegetation (Meroni et al., 2009). As fluorescence is competing with photochemical conversion, it may allow a more correct estimate of the carbon assimilation (Entcheva Campbell et al., 2008). Earth observation data for estimating fluorescence should have very high spectral resolution (0.05–0.1 nm) due to its narrow features, but considering the rapid technical development within sensors for hyperspectral measurements, fluorescence possibly has strong practical potential for monitoring vegetation status (Meroni et al., 2009; Entcheva Campbell et al., 2008). Globally mapped terrestrial chlorophyll fluorescence retrievals are already produced from the GOME-2 instrument at a spatial resolution of $0.5^\circ \times 0.5^\circ$, but hopefully this will be available also with EO sensors of higher spatial and temporal resolution in the future (Joiner et al., 2013).

The strongest wavelength combinations for estimating LUE for this semi-arid ecosystem was NDSI[688, 435]. The 688 nm wavelength is just at the base of the

red edge region, again indicating the importance of this spectral region for estimating photosynthetic activity. The wavelength at 435 nm is at the center of the blue range characterized by chlorophyll utilization, and strongly related to chlorophyll *a* and *b*, senescing, carotenoid, loss of chlorophyll, and vegetation browning (Thenkabail et al., 2004, 2012). The NDSI[688, 435] thereby explores the difference between information about chlorophyll content and information about senescence of the vegetation, which should be a good predictor of photosynthetic efficiency.

4.2.4 FAPAR

FAPAR is an estimate of radiation absorption in the photosynthetically active spectrum and thereby strongly negatively correlated to most parts of the reflectance spectrum (Fig. 5d). FAPAR remained high during the dry season because of standing dry biomass that was slowly degrading over the dry season (Fig. 2g). The seasonal dynamics in FAPAR is thereby strongly related to senescence of the vegetation, which explains why FAPAR was most strongly correlated to blue wavelengths (ρ_{412}). Several studies reported a strong relationship between NDVI and FAPAR (e.g. Tagesson et al., 2012; Myneni and Williams, 1994; Fensholt et al., 2004), but this relationship has been shown to vary for the vegetative phase and the periods of senescence (Inoue et al., 1998; Tagesson et al., 2014). As showed by Inoue et al. (2008), and confirmed by this study, new indices combining blue with NIR wavelengths could be used for estimating FAPAR for the entire phenological cycle. This result has implications for studies using the LUE approach for estimating C assimilations (Hilker et al., 2008).

4.3 Outlook and perspectives

Very limited multi-angular hyperspectral in situ data exists, even though it has been, and will continue to be extremely valuable for an improved understanding of the interaction between ground surface properties and radiative transfer. In this study, we have presented a unique in situ dataset of multi-angular, high temporal

BGD

12, 3315–3347, 2015

Hyperspectral reflectance of semi-arid savannas

T. Tagesson et al.

Title Page

Abstract

Introduction

Conclusions

References

Tables

Figures



Back

Close

Full Screen / Esc

Printer-friendly Version

Interactive Discussion



Hyperspectral reflectance of semi-arid savannas

T. Tagesson et al.

Title Page

Abstract

Introduction

Conclusions

References

Tables

Figures



Back

Close

Full Screen / Esc

Printer-friendly Version

Interactive Discussion



resolution hyperspectral reflectance (350–1800 nm) and demonstrated the applicability of hyperspectral data for estimating ground surface properties of semi-arid savanna ecosystems using NDSI. The study was conducted in spatially homogeneous savanna grassland, suggesting that the results should be commonly applicable for this biome type. However, attention should be paid to site-specific details that could affect the indices, such as species composition, soil type, biotic and abiotic stresses, and stand structure. Additionally, the biophysical mechanisms behind the NDSIs are not well understood at the moment, and further studies are needed to examine the applicability of these indices to larger regions and other ecosystems. Being a 2-band ratio approach, NDSI does not take full advantage of exploring the rich information given by the hyperspectral reflectance measurements. In the future, this hyperspectral reflectance data-set could be fully explored using e.g. derivative techniques, multivariate methods, and creation, parameterisation and evaluation of bidirectional reflectance distribution functions and radiative transfer models.

Even though several other methods exist which fully exploit the information in the hyperspectral reflectance spectrum, results of the present study still indicate the strength of normalised difference indices for extrapolating seasonal dynamics in properties of savanna ecosystems. A number of wavelengths in the reflectance spectra that are highly correlated to seasonal dynamics in properties of semiarid savanna ecosystems have been identified. The relationships between NDSI and ecosystem properties were better determined, or at the same level, as results of previous studies exploring relationships between hyperspectral reflectance and ecosystem properties (Kumar, 2007; Cho et al., 2007; Mutanga and Skidmore, 2004; Psomas et al., 2011; Ide et al., 2010). By studying also the impact from varying viewing and illumination geometry the feasibility and applicability of using indices for up-scaling to EO data was evaluated. As such, the results presented here offer insights for assessment of ecosystem properties using EO data and this information could be used for designing future sensors for observation of ecosystem properties of the Earth.

Acknowledgements. This paper was written within the frame of the project entitled Earth Observation based Vegetation productivity and Land Degradation Trends in Global Drylands. The project was funded by the Danish Council for Independent Research (DFF) Sapere Aude programme. The site is maintained by the Centre de Recherches Zootechniques de Dahra, Institut Sénégalais de Recherches Agricoles (ISRA).



This publication is supported
by COST – www.cost.eu

References

- Asner, G. P.: Biophysical and biochemical sources of variability in canopy reflectance, *Remote Sens. Environ.*, 64, 234–253, doi:10.1016/S0034-4257(98)00014-5, 1998.
- Bicheron, P. and Leroy, M.: Bidirectional reflectance distribution function signatures of major biomes observed from space, *J. Geophys. Res.-Atmos.*, 105, 26669–26681, doi:10.1029/2000JD900380, 2000.
- Bowyer, P. and Danson, F. M.: Sensitivity of spectral reflectance to variation in live fuel moisture content at leaf and canopy level, *Remote Sens. Environ.*, 92, 297–308, doi:10.1016/j.rse.2004.05.020, 2004.
- Ceccato, P., Gobron, N., Flasse, S., Pinty, B., and Tarantola, S.: Designing a spectral index to estimate vegetation water content from remote sensing data: Part 1: Theoretical approach, *Remote Sens. Environ.*, 82, 188–197, doi:10.1016/S0034-4257(02)00037-8, 2002.
- Cho, M. A., Skidmore, A., Corsi, F., van Wieren, S. E., and Sobhan, I.: Estimation of green grass/herb biomass from airborne hyperspectral imagery using spectral indices and partial least squares regression, *Int. J. Appl. Earth Obs.*, 9, 414–424, doi:10.1016/j.jag.2007.02.001, 2007.
- Cihlar, J., Manak, D., and Voisin, N.: AVHRR bidirectional reflectance effects and compositing, *Remote Sens. Environ.*, 48, 77–88, doi:10.1016/0034-4257(94)90116-3, 1994.
- Coburn, C. A. and Peddle, D. R.: A low-cost field and laboratory goniometer system for estimating hyperspectral bidirectional reflectance, *Can. J. Remote Sens.*, 32, 244–253, doi:10.5589/m06-021, 2006.

BGD

12, 3315–3347, 2015

Hyperspectral reflectance of semi-arid savannas

T. Tagesson et al.

[Title Page](#)

[Abstract](#)

[Introduction](#)

[Conclusions](#)

[References](#)

[Tables](#)

[Figures](#)



[Back](#)

[Close](#)

[Full Screen / Esc](#)

[Printer-friendly Version](#)

[Interactive Discussion](#)



Hyperspectral reflectance of semi-arid savannas

T. Tagesson et al.

[Title Page](#)

[Abstract](#)

[Introduction](#)

[Conclusions](#)

[References](#)

[Tables](#)

[Figures](#)



[Back](#)

[Close](#)

[Full Screen / Esc](#)

[Printer-friendly Version](#)

[Interactive Discussion](#)



Danson, F. M., Steven, M. D., Malthus, T. J., and Clark, J. A.: High-spectral resolution data for determining leaf water content, *Int. J. Remote Sens.*, 13, 461–470, doi:10.1080/01431169208904049, 1992.

Entcheva Campbell, P. K., Middleton, E. M., Corp, L. A., and Kim, M. S.: Contribution of chlorophyll fluorescence to the apparent vegetation reflectance, *Sci. Total Environ.*, 404, 433–439, doi:10.1016/j.scitotenv.2007.11.004, 2008.

Falge, E., Baldocchi, D., Olson, R., Anthoni, P., Aubinet, M., Bernhofer, C., Burba, G., Ceulemans, R., Clement, R., Dolman, H., Granier, A., Gross, P., Grunwald, T., Hollinger, D., Jensen, N. O., Katul, G., Keronen, P., Kowalski, A., Lai, C. T., Law, B. E., Meyers, T., Moncrieff, J., Moors, E., Munger, J. W., Pilegaard, K., Rannik, U., Rebmann, C., Suyker, A., Tenhunen, J., Tu, K., Verma, S., Vesala, T., Wilson, K., and Wofsy, S.: Gap filling strategies for defensible annual sums of net ecosystem exchange, *Agr. Forest Meteorol.*, 107, 43–69, 2001.

Fensholt, R., Sandholt, I., and Rasmussen, M. S.: Evaluation of MODIS LAI, fAPAR and the relation between fAPAR and NDVI in a semi-arid environment using in situ measurements, *Remote Sens. Environ.*, 91, 490–507, doi:10.1016/j.rse.2004.04.009, 2004.

Fensholt, R., Sandholt, I., and Stisen, S.: Evaluating MODIS, MERIS, and VEGETATION vegetation indices using in situ measurements in a semiarid environment, *IEEE T. Geosci. Remote*, 44, 1774–1786, doi:10.1109/TGRS.2006.875940, 2006.

Fensholt, R., Sandholt, I., Proud, S. R., Stisen, S., and Rasmussen, M. O.: Assessment of MODIS sun-sensor geometry variations effect on observed NDVI using MSG SEVIRI geostationary data, *Int. J. Remote Sens.*, 31, 6163–6187, 2010.

Feret, J.-B., François, C., Asner, G. P., Gitelson, A. A., Martin, R. E., Bidel, L. P. R., Ustin, S. L., le Maire, G., and Jacquemoud, S.: PROSPECT-4 and 5: Advances in the leaf optical properties model separating photosynthetic pigments, *Remote Sens. Environ.*, 112, 3030–3043, doi:10.1016/j.rse.2008.02.012, 2008.

Gamon, J. A., Peñuelas, J., and Field, C. B.: A narrow-waveband spectral index that tracks diurnal changes in photosynthetic efficiency, *Remote Sens. Environ.*, 41, 35–44, doi:10.1016/0034-4257(92)90059-S, 1992.

Gao, F., Jin, Y., Schaaf, C. B., and Strahler, A. H.: Bidirectional NDVI and atmospherically resistant BRDF inversion for vegetation canopy, *IEEE T. Geosci. Remote*, 40, 1269–1278, doi:10.1109/TGRS.2002.800241, 2002.

Hyperspectral reflectance of semi-arid savannas

T. Tagesson et al.

[Title Page](#)

[Abstract](#)

[Introduction](#)

[Conclusions](#)

[References](#)

[Tables](#)

[Figures](#)



[Back](#)

[Close](#)

[Full Screen / Esc](#)

[Printer-friendly Version](#)

[Interactive Discussion](#)



- Gates, D. M., Keegan, H. J., Schleter, J. C., and Weidner, V. R.: Spectral properties of plants, *Appl. Optics*, 4, 11–20, 1965.
- Gitelson, A. A., Merzlyak, M. N., and Lichtenthaler, H. K.: Detection of red edge position and chlorophyll content by reflectance measurements near 700 nm, *J. Plant Physiol.*, 148, 501–508, doi:10.1016/S0176-1617(96)80285-9, 1996.
- 5 Gower, S. T., Kucharik, C. J., and Norman, J. M.: Direct and indirect estimation of leaf area index, fAPAR, and net primary production of terrestrial ecosystems – a real or imaginary problem?, *Remote Sens. Environ.*, 70, 29–51, 1999.
- Hapke, B., DiMucci, D., Nelson, R., and Smythe, W.: The cause of the hot spot in vegetation canopies and soils: shadow-hiding versus coherent backscatter, *Remote Sens. Environ.*, 58, 63–68, doi:10.1016/0034-4257(95)00257-X, 1996.
- 10 Hilker, T., Coops, N. C., Wulder, M. A., Black, T. A., and Guy, R. D.: The use of remote sensing in light use efficiency based models of gross primary production: a review of current status and future requirements, *Sci. Total Environ.*, 404, 411–423, doi:10.1016/j.scitotenv.2007.11.007, 2008.
- 15 Holben, B. and Fraser, R. S.: Red and near-infrared sensor response to off-nadir viewing, *Int. J. Remote Sens.*, 5, 145–160, doi:10.1080/01431168408948795, 1984.
- Huber, S., Tagesson, T., and Fensholt, R.: An automated field spectrometer system for studying VIS, NIR and SWIR anisotropy for semi-arid savanna, *Remote Sens. Environ.*, 152, 547–556, 2014.
- 20 Huete, A. R., Hua, G., Qi, J., Chehbouni, A., and van Leeuwen, W. J. D.: Normalization of multidirectional red and NIR reflectances with the SAVI, *Remote Sens. Environ.*, 41, 143–154, doi:10.1016/0034-4257(92)90074-T, 1992.
- Ide, R., Nakaji, T., and Oguma, H.: Assessment of canopy photosynthetic capacity and estimation of GPP by using spectral vegetation indices and the light-response function in a larch forest, *Agr. Forest Meteorol.*, 150, 389–398, 2010.
- 25 Inoue, Y., Moran, M. S., and Horie, T.: Analysis of spectral measurements in rice paddies for predicting rice growth and yield based on a simple crop simulation model, *Plant Prod. Sci.*, 1, 269–279, 1998.
- 30 Inoue, Y., Penuelas, J., Miyata, A., and Mano, M.: Normalized difference spectral indices for estimating photosynthetic efficiency and capacity at a canopy scale derived from hyperspectral and CO₂ flux measurements in rice, *Remote Sens. Environ.*, 112, 156–172, 2008.

Hyperspectral reflectance of semi-arid savannas

T. Tagesson et al.

Title Page

Abstract

Introduction

Conclusions

References

Tables

Figures



Back

Close

Full Screen / Esc

Printer-friendly Version

Interactive Discussion



Jacquemoud, S., Verhoef, W., Baret, F., Bacour, C., Zarco-Tejada, P. J., Asner, G. P., François, C., and Ustin, S. L.: PROSPECT+SAIL models: a review of use for vegetation characterization, *Remote Sens. Environ.*, 113, S56–S66, doi:10.1016/j.rse.2008.01.026, 2009.

Jin, H. and Eklundh, L.: A physically based vegetation index for improved monitoring of plant phenology, *Remote Sens. Environ.*, 152, 512–525, doi:10.1016/j.rse.2014.07.010, 2014.

Jin, Y., Gao, F., Schaaf, C. B., Xiaowen, L., Strahler, A. H., Bruegge, C. J., and Martonchik, J. V.: Improving MODIS surface BRDF/Albedo retrieval with MISR multiangle observations, *IEEE T. Geosci. Remote*, 40, 1593–1604, doi:10.1109/TGRS.2002.801145, 2002.

Joiner, J., Guanter, L., Lindstrot, R., Voigt, M., Vasilkov, A. P., Middleton, E. M., Huemmrich, K. F., Yoshida, Y., and Frankenberg, C.: Global monitoring of terrestrial chlorophyll fluorescence from moderate-spectral-resolution near-infrared satellite measurements: methodology, simulations, and application to GOME-2, *Atmos. Meas. Tech.*, 6, 2803–2823, doi:10.5194/amt-6-2803-2013, 2013.

Kimes, D. S.: Dynamics of directional reflectance factor distributions for vegetation canopies, *Appl. Optics*, 22, 1364–1372, 1983.

Kumar, L.: High-spectral resolution data for determining leaf water content in Eucalyptus species: leaf level experiments, *Geocarto International*, 22, 3–16, 2007.

Lasslop, G., Reichstein, M., and Papale, D.: Separation of net ecosystem exchange into assimilation and respiration using a light response curve approach: critical issues and global evaluation, *Glob. Change Biol.*, 16, 187–209, 2010.

Lee, K., Cohen, W. B., Kennedy, R. E., Maersperger, T. K., and Gower, S. T.: Hyperspectral versus multispectral data for estimating leaf area index in four different biomes, *Remote Sens. Environ.*, 91, 508–520, 2004.

Mbow, C., Fensholt, R., Rasmussen, K., and Diop, D.: Can vegetation productivity be derived from greenness in a semi-arid environment? Evidence from ground-based measurements, *J. Arid Environ.*, 97, 56–65, doi:10.1016/j.jaridenv.2013.05.011, 2013.

Meroni, M., Rossini, M., Guanter, L., Alonso, L., Rascher, U., Colombo, R., and Moreno, J.: Remote sensing of solar-induced chlorophyll fluorescence: review of methods and applications, *Remote Sens. Environ.*, 113, 2037–2051, doi:10.1016/j.rse.2009.05.003, 2009.

Mutanga, O. and Skidmore, A. K.: Narrow band vegetation indices overcome the saturation problem in biomass estimation, *Int. J. Remote Sens.*, 25, 3999–4014, doi:10.1080/01431160310001654923, 2004.

Hyperspectral reflectance of semi-arid savannas

T. Tagesson et al.

[Title Page](#)

[Abstract](#)

[Introduction](#)

[Conclusions](#)

[References](#)

[Tables](#)

[Figures](#)



[Back](#)

[Close](#)

[Full Screen / Esc](#)

[Printer-friendly Version](#)

[Interactive Discussion](#)



- Myneni, R. B. and Williams, D. L.: On the relationship between FAPAR and NDVI, *Remote Sens. Environ.*, 49, 200–211, 1994.
- Pisek, J., Ryu, Y., Sprintsin, M., He, L., Oliphant, A. J., Korhonen, L., Kuusk, J., Kuusk, A., Bergstrom, R., Verrelst, J., and Alikas, K.: Retrieving vegetation clumping index from Multi-angle Imaging SpectroRadiometer (MISR) data at 275 m resolution, *Remote Sens. Environ.*, 138, 126–133, doi:10.1016/j.rse.2013.07.014, 2013.
- Psomas, A., Kneubühler, M., Huber, S., Itten, K., and Zimmermann, N. E.: Hyperspectral remote sensing for estimating aboveground biomass and for exploring species richness patterns of grassland habitats, *Int. J. Remote Sens.*, 32, 9007–9031, doi:10.1080/01431161.2010.532172, 2011.
- Qi, J., Chehbouni, A., Huete, A. R., Kerr, Y. H., and Sorooshian, S.: A modified soil adjusted vegetation index, *Remote Sens. Environ.*, 48, 119–126, 1994.
- Rasmussen, M. O., Götsche, F. M., Diop, D., Mbow, C., Olesen, F. S., Fensholt, R., and Sandholt, I.: Tree survey and allometric models for tiger bush in northern Senegal and comparison with tree parameters derived from high resolution satellite data, *Int. J. Appl. Earth Obs.*, 13, 517–527, doi:10.1016/j.jag.2011.01.007, 2011.
- Richter, K., Atzberger, C., Hank, T. B., and Mauser, W.: Derivation of biophysical variables from Earth observation data: validation and statistical measures, *J. Appl. Remote Sens.*, 61, 063557, doi:10.1117/1.JRS.6.063557, 2012.
- Roberto, C., Lorenzo, B., Michele, M., Micol, R., and Cinzini, P.: Optical remote sensing of vegetation water content, in: *Hyperspectral Remote Sensing of Vegetation*, edited by: Thenkabail, P. S., Lyon, J. G., and Huete, A., CRC Press, Taylor and Francis Group, Boca Raton, FL, 227–244, 2012.
- Rouse, J. W., Haas, R. H., Schell, J. A., Deering, D. W., and Harlan, J. C.: *Monitoring the Vernal Advancement of Retrogradation of Natural Vegetation, Type III, Final Report*, NASA/GSFC Greenbelt, MD, 1974.
- Sandmeier, S., Müller, C., Hosgood, B., and Andreoli, G.: Physical mechanisms in hyperspectral BRDF data of grass and watercress, *Remote Sens. Environ.*, 66, 222–233, doi:10.1016/S0034-4257(98)00060-1, 1998.
- Sims, D. A. and Gamon, J. A.: Estimation of vegetation water content and photosynthetic tissue area from spectral reflectance: a comparison of indices based on liquid water and chlorophyll absorption features, *Remote Sens. Environ.*, 84, 526–537, 2003.

Hyperspectral reflectance of semi-arid savannas

T. Tagesson et al.

Title Page

Abstract

Introduction

Conclusions

References

Tables

Figures



Back

Close

Full Screen / Esc

Printer-friendly Version

Interactive Discussion



Sjöström, M., Ardö, J., Eklundh, L., El-Tahir, B. A., El-Khidir, H. A. M., Hellström, M., Pilesjö, P., and Seaquist, J.: Evaluation of satellite based indices for gross primary production estimates in a sparse savanna in the Sudan, *Biogeosciences*, 6, 129–138, doi:10.5194/bg-6-129-2009, 2009.

5 Soudani, K., Hmimina, G., Dufrêne, E., Berveiller, D., Delpierre, N., Ourcival, J.-M., Rambal, S., and Joffre, R.: Relationships between photochemical reflectance index and light-use efficiency in deciduous and evergreen broadleaf forests, *Remote Sens. Environ.*, 144, 73–84, 2014.

10 Tagesson, T., Eklundh, L., and Lindroth, A.: Applicability of leaf area index products for boreal regions of Sweden, *Int. J. Remote Sens.*, 30, 5619–5632, 2009.

Tagesson, T., Mastepanov, M., Tamstorf, M. P., Eklundh, L., Schubert, P., Ekberg, A., Sigsgaard, C., Christensen, T. R., and Ström, L.: High-resolution satellite data reveal an increase in peak growing season gross primary production in a high-Arctic wet tundra ecosystem 1992–2008, *Int. J. Appl. Earth Obs.*, 18, 407–416, 2012.

15 Tagesson, T., Fensholt, R., Guiro, I., Rasmussen, M. O., Huber, S., Mbow, C., Garcia, M., Horion, S., Sandholt, I., Holm-Rasmussen, B., Götsche, F. M., Ridler, M.-E., Olén, N., Olsen, J. L., Ehammer, A., Madsen, M., Olesen, F. S., and Ardö, J.: Ecosystem properties of semi-arid savanna grassland in West Africa and its relationship to environmental variability, *Glob. Change Biol.*, 21, 250–264, doi:10.1111/gcb.12734, 2014.

20 Thenkabail, P. S., Smith, R. B., and De Pauw, E.: Hyperspectral vegetation indices and their relationships with agricultural crop characteristics, *Remote Sens. Environ.*, 71, 158–182, doi:10.1016/S0034-4257(99)00067-X, 2000.

25 Thenkabail, P. S., Enclona, E. A., Ashton, M. S., and Van Der Meer, B.: Accuracy assessments of hyperspectral waveband performance for vegetation analysis applications, *Remote Sens. Environ.*, 91, 354–376, 2004.

Thenkabail, P. S., Lyon, J. G., and Huete, A.: *Hyperspectral Remote Sensing of Vegetation*, CRC Press, Taylor and Francis Group, Boca Raton, FL, 705 pp., 2012.

Tucker, C. J.: Red and photographic infrared linear combinations for monitoring vegetation, *Remote Sens. Environ.*, 8, 127–150, doi:10.1016/0034-4257(79)90013-0, 1979.

30 van Leeuwen, W. J. D., Huete, A. R., and Laing, T. W.: MODIS vegetation index compositing approach: a prototype with AVHRR data, *Remote Sens. Environ.*, 69, 264–280, doi:10.1016/S0034-4257(99)00022-X, 1999.

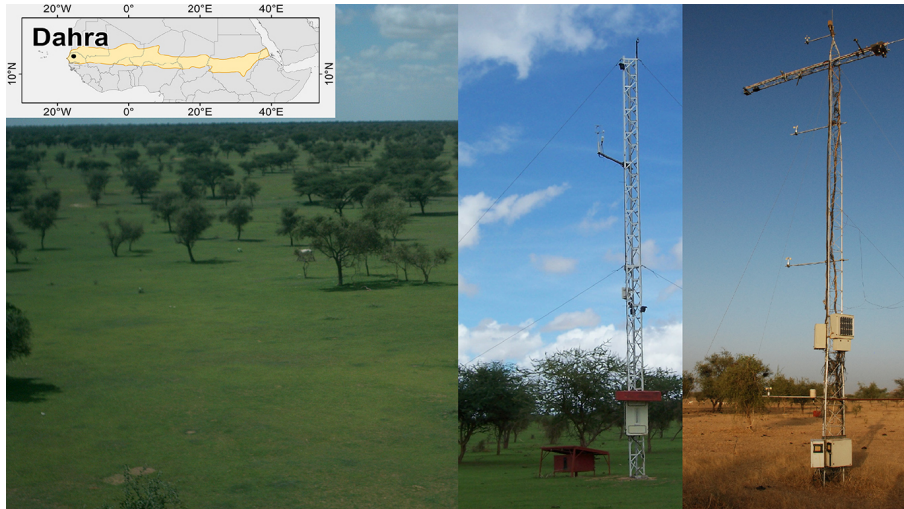


Figure 1. Overview picture of the measured area, and tower set-up for the eddy covariance tower (left), and the meteorological tower with the spectroradiometers (right). The overview picture and the picture of the eddy covariance tower show the rainy season whereas the picture of the meteorological tower shows the dry season. The map shows the location of Dahra within the Sahel (orange area).

BGD

12, 3315–3347, 2015

Hyperspectral reflectance of semi-arid savannas

T. Tagesson et al.

[Title Page](#)

[Abstract](#)

[Introduction](#)

[Conclusions](#)

[References](#)

[Tables](#)

[Figures](#)

◀

▶

◀

▶

[Back](#)

[Close](#)

[Full Screen / Esc](#)

[Printer-friendly Version](#)

[Interactive Discussion](#)



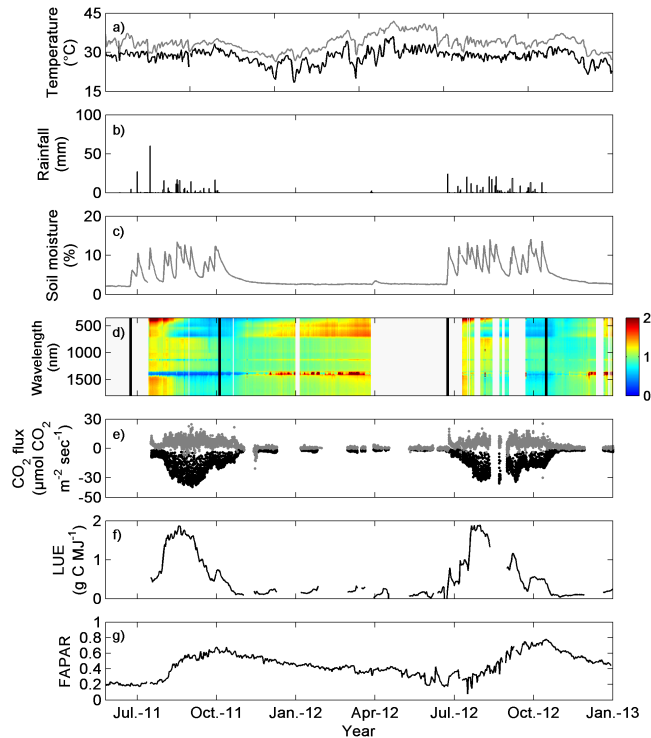


Figure 2. Time series of the measured variables: **(a)** daily averaged air temperature (black line), and soil temperature at 0.05 m depth (grey line), **(b)** daily sums of rainfall, **(c)** daily average of soil moisture at 0.05 m depth, **(d)** hyperspectral reflectance normalized by calculating the ratio between daily median reflectance for each wavelength (350–1800 nm) and the average reflectance for the entire measurement period, **(e)** gross primary productivity (GPP) (black dots) and ecosystem respiration (grey dots), **(f)** the light use efficiency (LUE), and **(g)** the fraction of photosynthetically active radiation absorbed by the vegetation (FAPAR). The black vertical lines are the start and end of the rainy seasons (first and final day of rainfall).

Hyperspectral reflectance of semi-arid savannas

T. Tagesson et al.

Title Page

Abstract Introduction

Conclusions References

Tables Figures

◀ ▶

◀ ▶

Back Close

Full Screen / Esc

Printer-friendly Version

Interactive Discussion



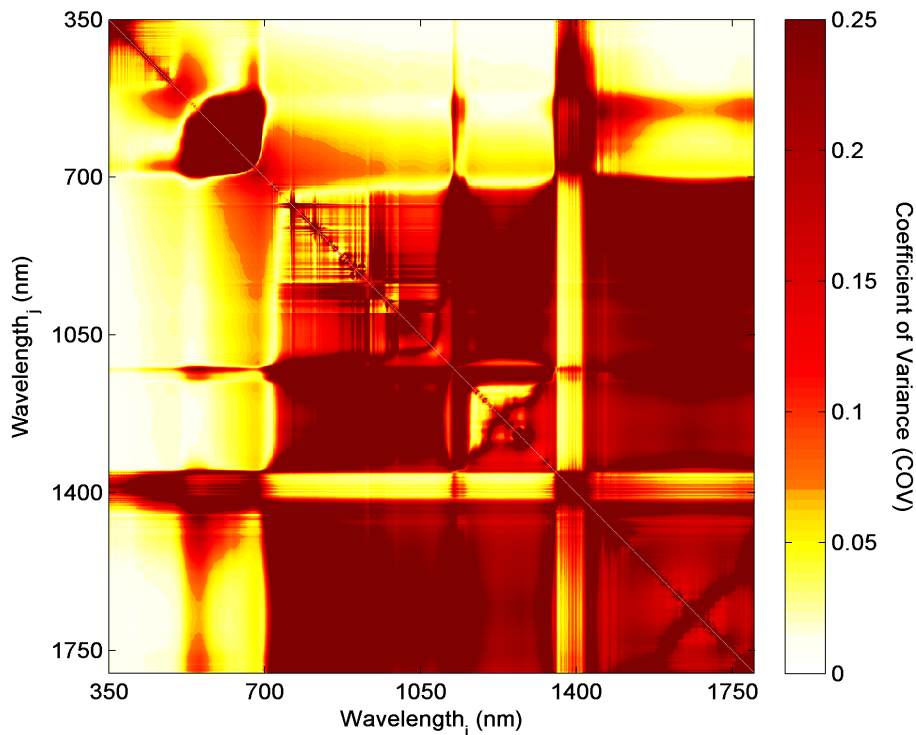


Figure 3. The coefficient of variation (COV), i.e. the ratio between daily SD and the daily mean (measurements taken between 8:00 and 18:00LT), for different NDSI wavelength ($\lambda_{i,j}$) combinations for 12 days at the peak of the growing season 2011 (day of year 237–251; $n = 576$). The COV indicates how strongly the NDSI are affected by variable sun angles.

Title Page

Abstract

Introduction

Conclusions

References

Tables

Figures



Back

Close

Full Screen / Esc

Printer-friendly Version

Interactive Discussion



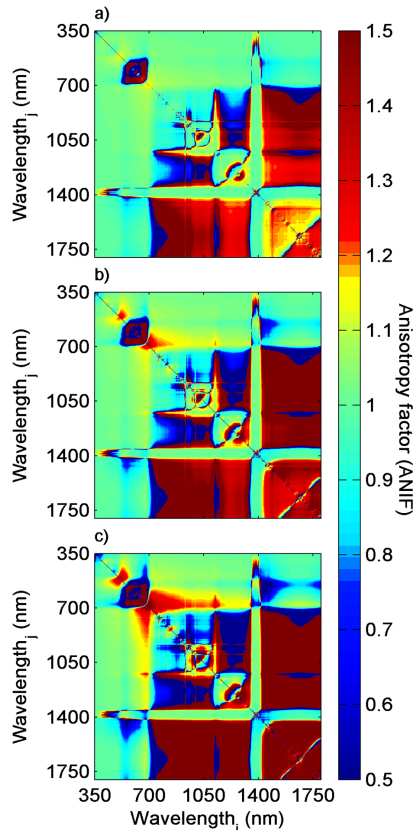


Figure 4. The anisotropy factor (ANIF) for different NDSI wavelength (i, j) combinations for 15 days at the peak of the growing season 2011 (day of year 237–251) for the different sensor viewing angles: **(a)** 15°, **(b)** 30°, and **(c)** 45°. The sensor is pointing east and west in the lower left and upper right corners of each plot, respectively. In order not to include effects of solar zenith angles in the analysis, only data measured between 12:00 and 14:00 LT were used in the ANIF calculations ($n = 48$).

Title Page

Abstract

Introduction

Conclusions

References

Tables

Figures



Back

Close

Full Screen / Esc

Printer-friendly Version

Interactive Discussion



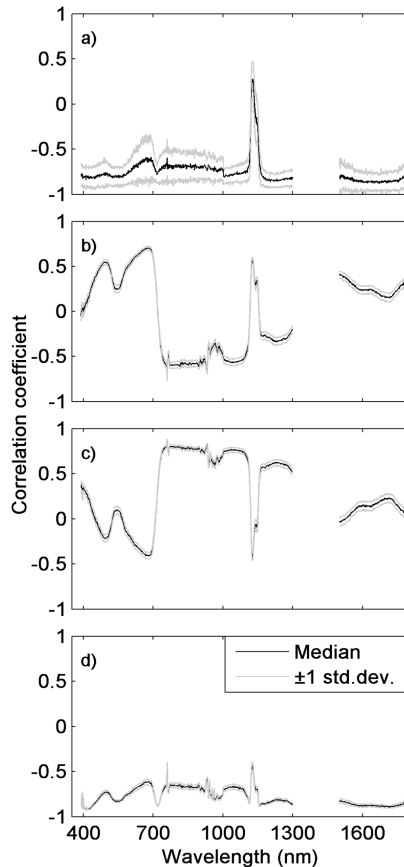


Figure 5. Median correlation coefficient (± 1 SD) between seasonal dynamics in hyperspectral reflectance 2011–2012 and **(a)** dry weight biomass ($n = 12$; g m^{-2}), **(b)** gross primary productivity (GPP) ($n = 285$; g C day^{-1}), **(c)** light use efficiency (LUE) ($n = 272$; g C MJ^{-1}), and **(d)** fraction of photosynthetically active radiation absorbed by the vegetation (FAPAR) ($n = 369$).

Hyperspectral reflectance of semi-arid savannas

T. Tagesson et al.

Title Page

Abstract

Introduction

Conclusions

References

Tables

Figures



Back

Close

Full Screen / Esc

Printer-friendly Version

Interactive Discussion



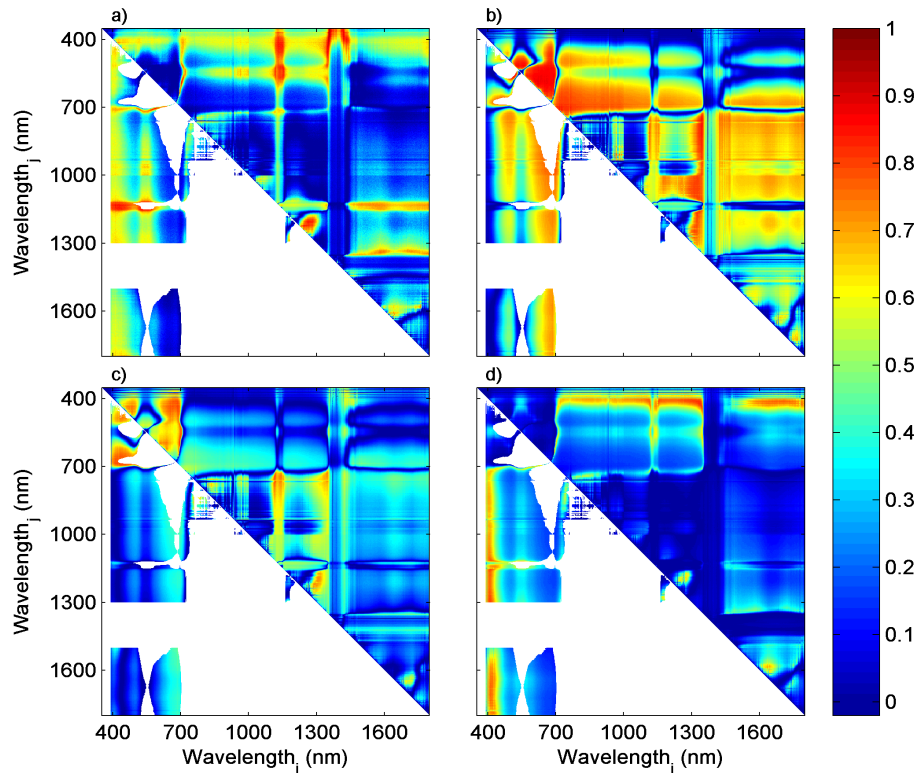


Figure 6. Coefficient of determination (R^2) between NDSI and **(a)** dry weight biomass ($n = 12$; g m^{-2}), **(b)** gross primary productivity (GPP) ($n = 285$; gC day^{-1}), **(c)** light use efficiency (LUE) ($n = 272$; gCMJ^{-1}), and **(d)** fraction of photosynthetically active radiation absorbed by the vegetation (FAPAR) ($n = 369$). The upper right half of each image shows the unfiltered R^2 values, whereas the lower left half shows filtered R^2 , based on the filtering criteria described under Sect. 2.6.

Title Page

Abstract

Introduction

Conclusions

References

Tables

Figures



Back

Close

Full Screen / Esc

Printer-friendly Version

Interactive Discussion



Hyperspectral
reflectance of
semi-arid savannas

T. Tagesson et al.

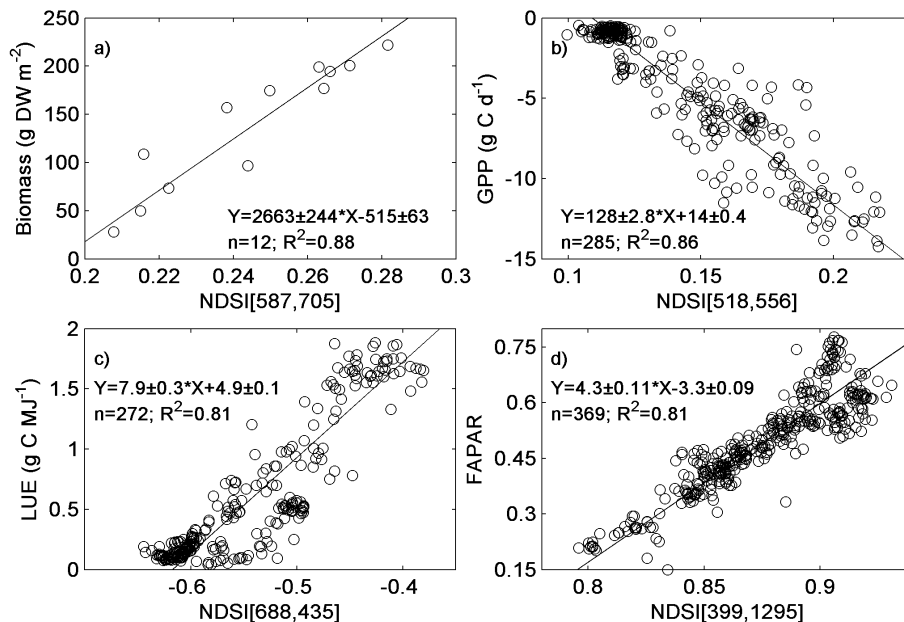


Figure 7. The least square linear regressions with the strongest relationships between the NDSI and **(a)** dry weight biomass, **(b)** gross primary productivity (GPP), **(c)** light use efficiency (LUE), and **(d)** fraction of photosynthetically active radiation absorbed by the vegetation (FAPAR). In the equations, the slope and intercepts (± 1 SD) is given.

Title Page

Abstract

Introduction

Conclusions

References

Tables

Figures



Back

Close

Full Screen / Esc

Printer-friendly Version

Interactive Discussion

